Solid Freeform Fabrication 2024: Proceedings of the 35th Annual International Solid Freeform Fabrication Symposium – An Additive Manufacturing Conference
Reviewed Paper

Research on influence of scan strategy on part shrinkage in low temperature laser sintering of polymer

T. Kigure*, Y. Yamauchi*, T. Niino†

*Tokyo Metropolitan Industrial Technology Research Institute
†Institute of Industrial Science, the University of Tokyo

Abstract

Low temperature laser sintering of polymer allows the powder bed temperature during the process to be set lower than the recrystallisation temperature. In previous studies, this process has achieved improvements in the material recycling rate. In addition, the processing of high-performance plastics in non-high temperature resistant machines have been achieved.

While general laser sintering is simultaneous solidification, low temperature laser sintering is sequential solidification layer by layer. Because of the different solidification processes, the shrinkage behavior and shape of the two are also different. Therefore, the shape correction method used in general laser sintering, which multiplies the pre-measured shrinkage rate, is not applicable to low temperature laser sintering, and it is necessary to construct a shape correction method for low temperature laser sintering. However, the behavior and mechanism of shrinkage in low temperature laser sintering are unknown, and this is a problem in constructing a shape correction method.

The goal of this study is to construct a shape correction method for low temperature laser sintering. As a first step, the fundamental phenomenon of shrinkage in the low temperature laser sintering was investigated. As a result, it was shown that the effect of scan strategy for shrinkage appeared in the lower part of the specimen, but it was mitigated in the middle and upper part of the specimen. These results provide basic information for understanding the shrinkage mechanism to construct the shape correction method for low temperature laser sintering.

Introduction

Laser sintering irradiate the laser selectively onto material powder bed to melt and solidify the material to create the parts. Since laser sintering can use crystalline thermoplastic that has generally chemical resistance as the feed material, and the built parts have high strength and high toughness in the polymer parts, it has expected as a manufacturing technology for mass products.

The molten polymer material shrinks as it solidifies. Part warpage during process due to shrinkage can be a cause of process failure. In a typical laser sintering process, the powder bed temperature is maintained between the melting temperature and the recrystallisation temperature to suppress warpage. In this temperature range, the molten material becomes a supercooling, which keeps the liquid phase even below the melting temperature [1]. This warpage suppression method has the advantage that no support structure is needed for the build. However, to use this method, the usable material is limited because the melting temperature and recrystallisation temperature of the material must be separated. In addition, thermal degradation progresses [2-4], which reduces the material recycling rate.

Low temperature laser sintering [5] is proposed as a method to solve these problems mentioned before. This process suppresses warpage during the process by anchoring the parts to a rigid base plate. Low temperature laser sintering can set any powder bed temperature during the process, including lower than the recrystallisation temperature. This characteristic is expected to expand the usable material and suppress thermal degradation of the material. I The following results have been achieved in previous studies. A recycling rate of 90% has been achieved for laser sintering of PA 12, which is higher than the typical recycling rates of 60 % or 70 % for typical laser sintering of it [6]. The process for PEEK, a high-performance plastic that normally requires a high temperature machine, was achieved by low temperature laser sintering using a commercially available non-high

temperature machine [7]. By setting different powder bed temperatures in low-temperature laser sintering, parts with different crystallinity have been produced [8].

The solidification process is different between typical laser sintering and low temperature laser sintering. In the typical laser sintering process, the supercooling is maintained after the top of layer is built, and solidification starts after the lamination process [9]. On the other hand, in low temperature laser sintering, the melted material is rapidly cooled and solidified by ambient temperatures below the recrystallization temperature. So that solidification occurs per layer building. Since shrinkage starts with solidification, the part shrinkage of low temperature laser sintering is not uniform. Therefore, the size expansion of input data which is same as typical laser sintering is not available as a correction method for low temperature laser sintering. For this reason, a new shape correction method specific to low temperature laser sintering is needed. However, the shrinkage mechanism and deformation tendency of the whole part are not yet known.

Our final goal is to obtain the desired shape by low-temperature laser sintering by predicting deformation due to shrinkage and correcting the input data. As a first step, the effect of scan strategy on the parts shape of low temperature laser sintering was investigated. Specimens were built by using three scan strategies, which are single scan single hatch, single scan reverse hatch and cross scan reverse hatch. After the building, the dimensional deviation from input data of parts was measured by 3D scanner. As a result, it was indicated that the effect of the scan strategy was clearly observed at low parts and it's decreased as the process progressed.

Methodology

Material and machine

The machine used in this study was commercial laser sintering machine RaFaEl300F (Aspect Inc.). This machine equips wavelength of 1.09μm fiber laser and workspace is 340×340×430mm.

The Material was PA11 based powder Aspex-FPA black (Aspect Inc.). The average powder particle size D_{50} was 50μm. The melting point, recrystallization temperature and glass transition temperature measured by DSC are 200℃ and 155℃, 50℃, respectively.

Build condition

The build parameters sets are shown in Table 1. The powder bed temperature was set at 70℃, which is between the glass transition temperature and the recrystallization temperature of the material. The energy per unit area was set at 0.01J/mm^2, which corresponds to the modified energy melt ratio (*Modified EMR*) of 2.5 for this material. The *Modified EMR* is an energy supply index proposed by Yamauchi et al, and is defined as the ratio of the input energy E_{vm} to the energy required to melt the powder E_{pm} as follows [10]:

$$Modified\ EMR = \frac{E_{vm}}{E_{pm}} = \frac{(1 - R_0 - R_{z_n}) \times \frac{P}{y \times v} \times \left(1 - e^{-\frac{z_n}{D_{pp}}}\right)}{[C_P(T_m - T_b) + h_f] \times (\rho)(\Phi) \times Z_n} \quad (1)$$

Where R_0, R_{z_n}, P, y, v, D_{pp}, C_P, T_m, T_b, h_f, ρ, Φ and Z_n denote the specular reflectance, diffuse reflectance for the powder layer thickness, laser power, hatch distance, scan speed, penetration depth of the powder material, specific heat capacity, melting point, powder bed temperature, heat of fusion, material density, powder packing ratio, and layer thickness, respectively.

Table 1 Build parameters set.

Spot diameters	Laser power	Hatching space	Scan speed	Powder bed temp.	Layering pitch
170 μm	10 W	0.05 mm	2000 mm/s	70 ℃	0.1mm

Figure 1 shows laser scan strategies. The hatching direction was defined as perpendicular to the scan direction. Three patterns of scan strategies were chosen. Single scan single hatch was that scan direction and hatching direction are same in all layers. Single scan reverse hatch was that scan direction was same in all layers and the hatching direction is switched layer by layer. Cross scan reverse hatch is that scan direction and hatching direction is rotated by 90° per layer. The laser beam offset, defined as the distance value from the design data to the laser scan to adjust the dimensions, was set to 0. No contour scan was performed, only a fill scan.

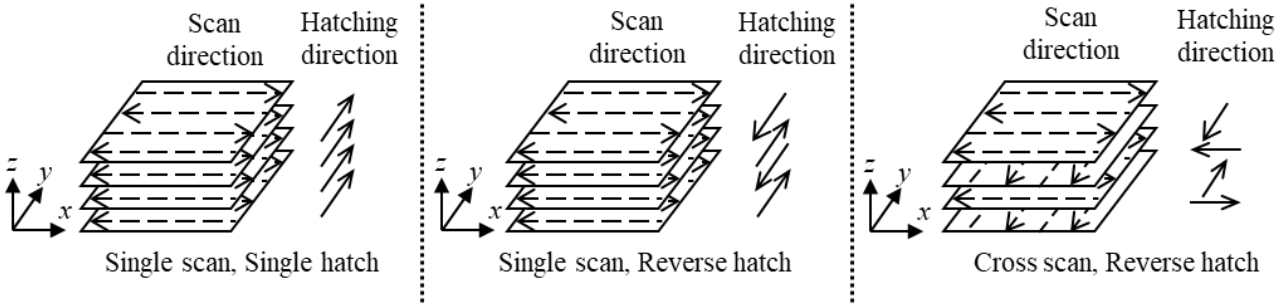

Figure 1. Scanning strategy and coordinate axis

Figure 2 shows input model data and dimensions. The cross section of the specimen was set to 10 × 10 mm and the height of the specimen was set to 1 mm, 5 mm and 10 mm. Support structure was designed in 1.5 × 1.5 × 5 mm.

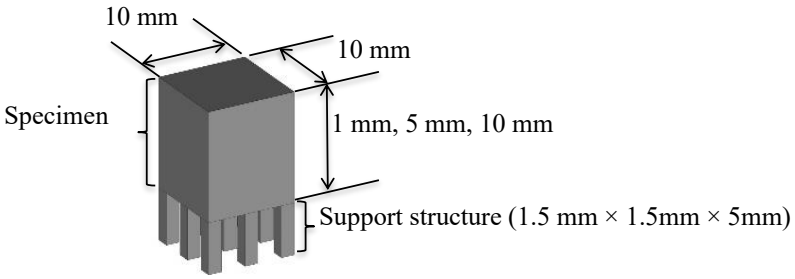

Figure2. shape of input model data.

Shape measurement condition

The 3D scanner FLARE Pro (Tokyo boeki techno systems LTD.) was used for shape measurement. Setting of 33μm resolution (FOV200) was selected. Multi angle measurements were performed using a rotary table to obtain overall shape data. The dimension and cross-sectional shape were obtained by dimensional measurement software SP-Gauge (Armonics co.LTD.). The shrinkage was calculated as follows, similar to other reports [11].

$$shrinkage = \frac{measured\ dimension - input\ data\ dimension}{input\ data\ dimension} \quad (2)$$

Experimental result

Figure 3 shows specimens in each scan strategy. In all the specimens the support structures were bent, and the specimens were deformed compared to the input data shown in Figure 2. The degree of bend of support structure was depended on scan strategies, the specimen of cross scan reverse hatch was lower than other two

scan strategies. In addition, regardless of the scan strategy, an overhanging was observed in the specimen thickness of 1 mm. The width of the specimen gradually increases upward in the other two heights.

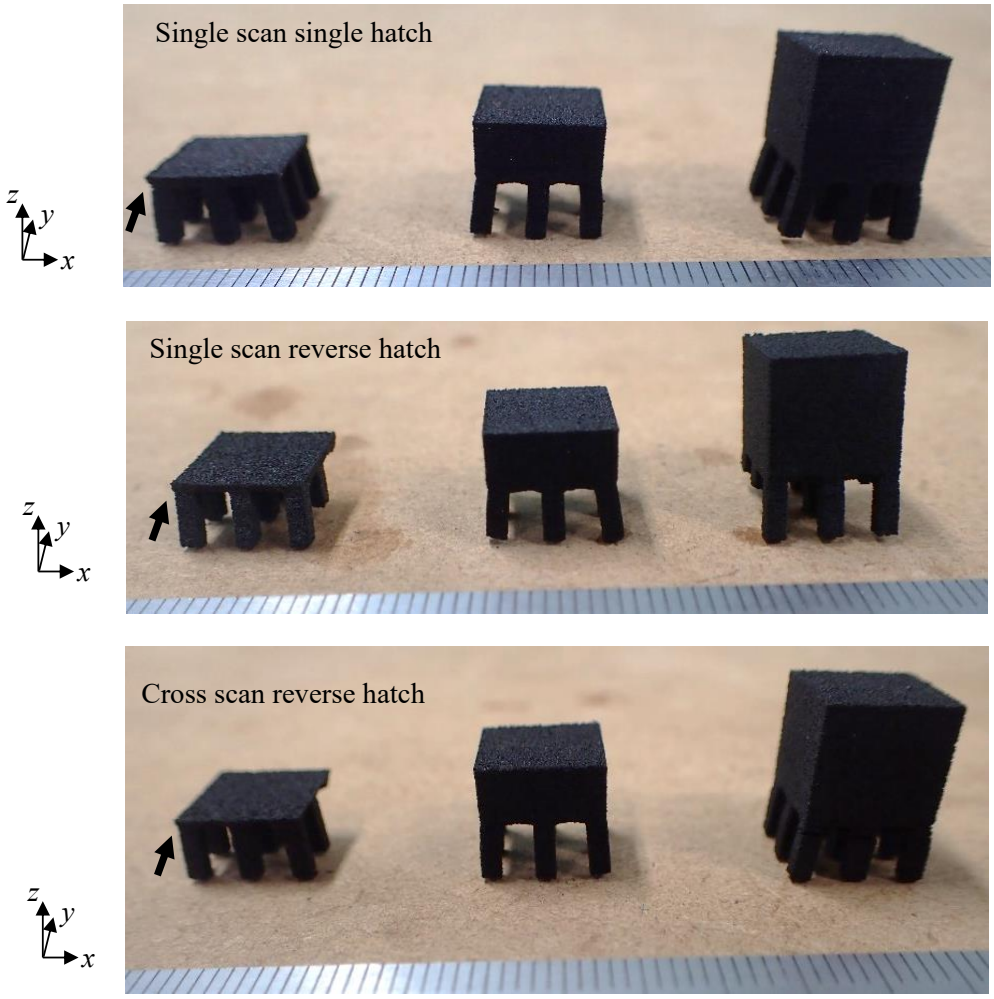

Figure 3. Specimens of each scan strategy.
Upper is single scan single hatch, middle is single scan reverse hatch, and lower is cross scan reverse hatch. The relationship between coordinate axis and direction of scan strategy is same as figure 1. Arrow indicates overhanging.

Figure 4 shows the results of shrinking behavior in the x -direction for the z-direction in each specimen. The shrinkage of all the specimens decreased with increasing of the z-position. In the specimens of 1 mm thickness, the shrinkage was different in each scan strategy. The shrinkage was smaller in the order of single scan single hatch, single scan reverse hatch, and cross scan reverse hatch. On the other hand, almost no scan strategy dependence was observed for specimens of 5 mm and 10 mm thickness.

Figure 5 shows the results of shrinking behavior in the y-direction for the z-direction in each specimen. The scan strategy dependence was observed for all results. The specimens of single scan reverse hatch showed the smallest shrinkage in all specimens of thickness. In the lower part of specimen ($Z > 0.7$mm), cross scan reverse hatch showed the largest shrinkage and opposite behavior with the result of the other two scan strategies. In the middle and upper part of specimen ($Z < 0.7$mm), the shrinking behavior of single scan single hatch and cross scan reverse hatch were almost the same.

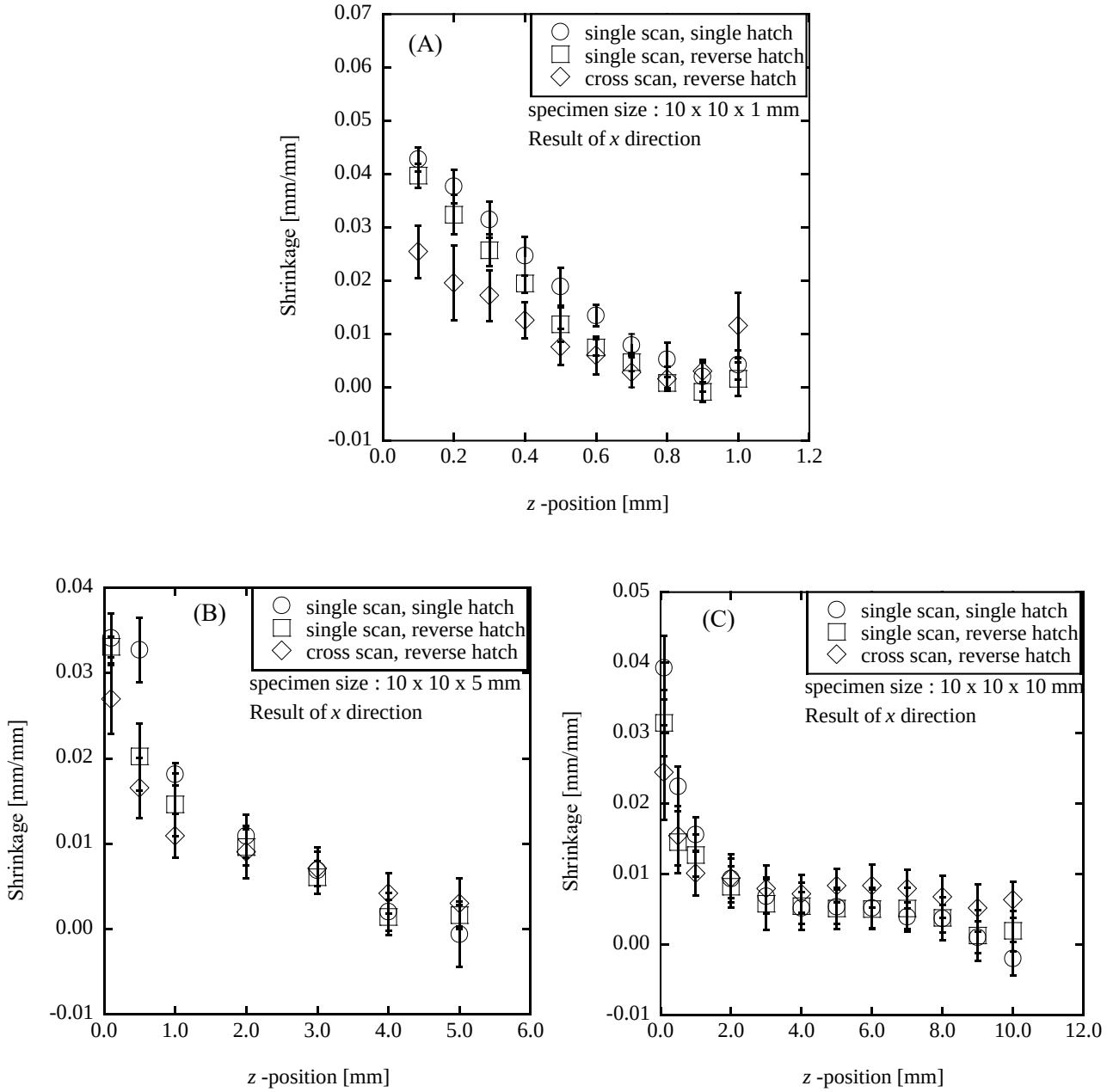

Figure 4. *z*-direction shrinkage behavior of *x*-direction in each specimen size.
(A) is 1mm thickness, (B) is 5 mm thickness, and (C) is 10 mm thickness. Same marker indicates same scan strategy.

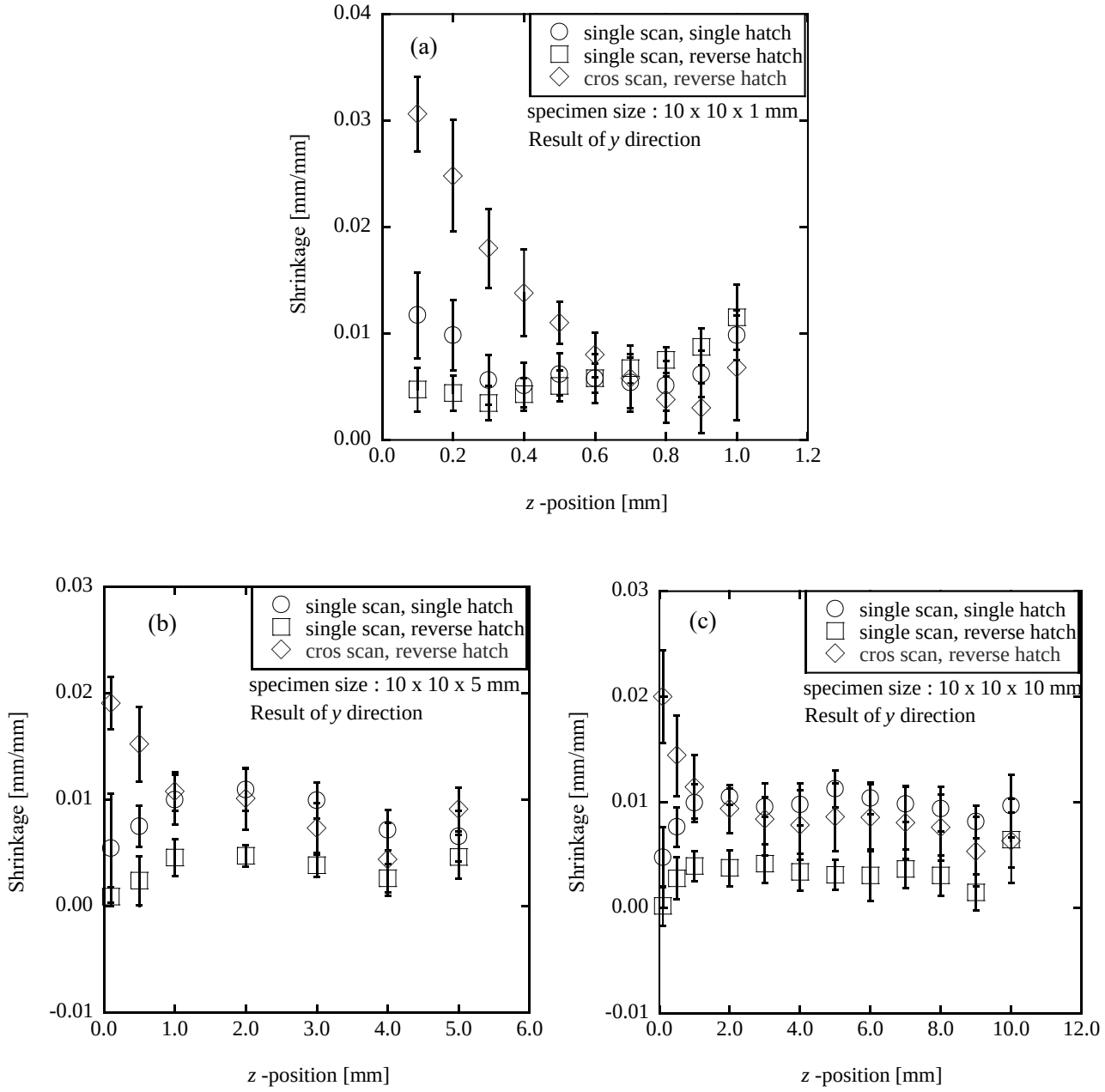

Figure 5. *z*-direction shrinkage behavior of *y*-direction in each specimen size.
(a) is 1mm thickness, (b) is 5 mm thickness, and (c) is 10 mm thickness. Same marker indicates same scan strategy.

Figure 6 shows the difference in shrinkage between *x*-direction and *y*-direction in specimen 10mm thickness. In the result of single scan single hatch, the *x*-direction shrinkage was larger than the *y*-direction shrinkage up to the 2mm height, but the *y*-direction shrinkage became larger than the *x*-direction shrinkage when the exceeded at 2mm height. In the result of single scan reverse hatch, the *x*-direction shrinkage is larger than that in the *y*-direction in all parts. In the result of cross scan reverse hatch, there was no direction dependence. In addition, the uniform behavior in the middle height of the specimens was shown in all scan strategies.

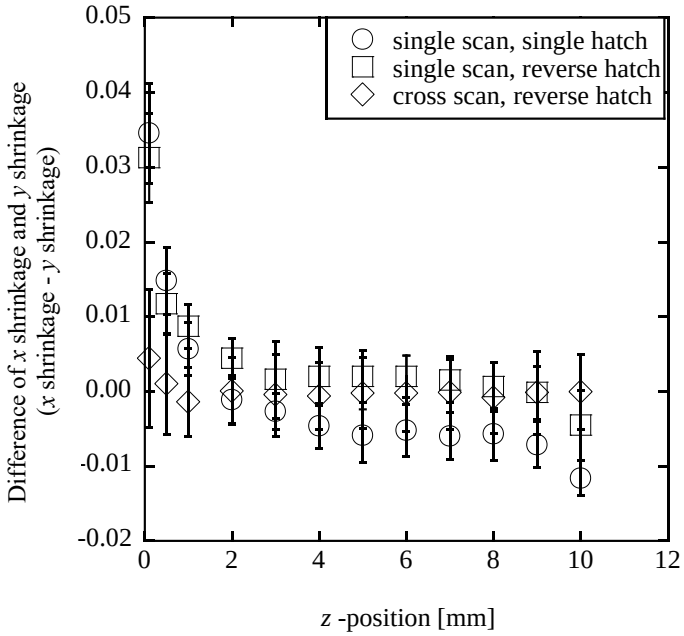

Figure 6. Difference of *x*-shrinkage and *y*-shrinkage in specimen of 10 mm thickness in each scan strategy.
Zero means shrinkage was isotropic, minas mean shrinkage of *y*-direction is larger than shrinkage of *x*-direction, and plus means shrinkage of *x*-direction is larger than shrinkage of *y*-direction.

The cross sections of the specimens for each scan strategy are shown in Figure 7. Focusing on the cross section at 0.1 mm height in each scan strategy, the single scan single hatch showed a rectangle with curved top and bottom side, single scan reverse hatch showed rectangle, and cross scan reverse hatch showed square. This trend remained height of 0.5mm, but this characteristic shape disappeared as the height exceeded 1.0mm. Regardless of the scan strategy, the cross section exceeded 1.0mm height approached a square.

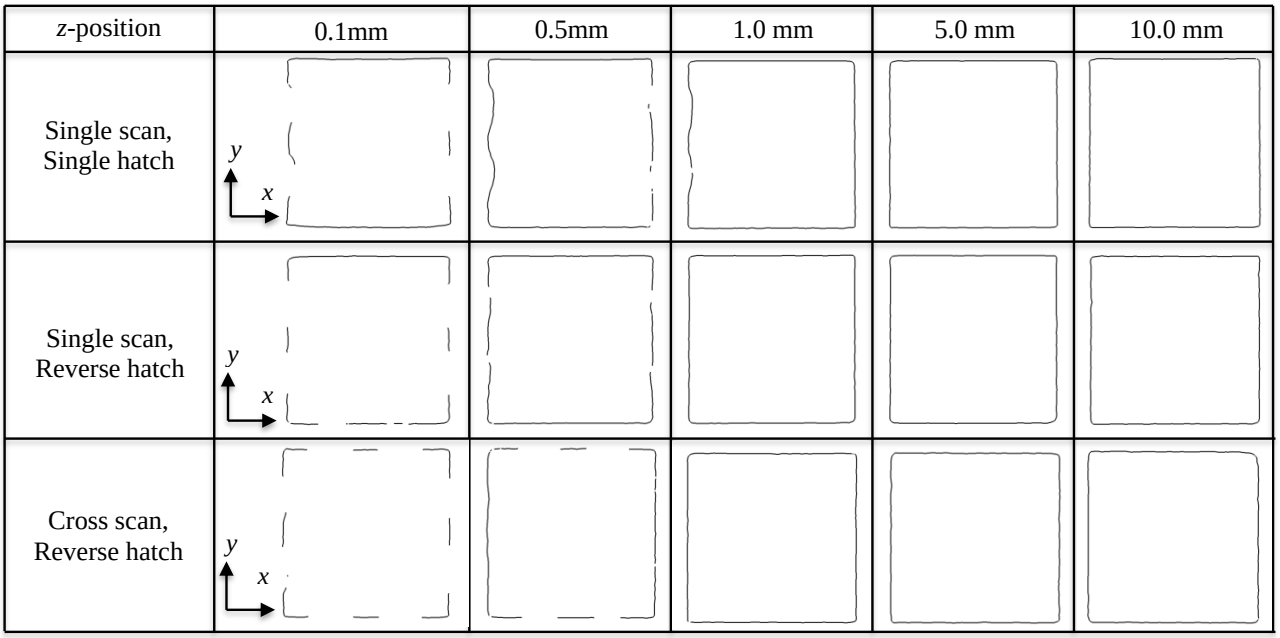

Figure 7. Cross section of specimen of 10 mm thickness in each *z*-position.

Discussion

The reason why the shrinkage in the low temperature sintering varies in the *z*-direction is due to the sequential solidification of melted material as in the powder bed fusion of metal [12]. In sequential solidification, the already built lower layers suppress the shrinkage of the newly built top layer. At the same time, lower layers receive compressive force from the newly built top layer. This compressive force causes the lower layers to shrink further. This process is repeated each time a new layer is built. As a result, as shown in Figure 4, the shrinkage is lowest at the top and the bottom shrinkage is largest. However, the *y*-direction shrinkage in Figure 5 is the smallest at the bottom, except for the cross scan reverse hatch. This can be assumed for two reasons. The first is that the shrinkage in the hatching direction is small, and the compressive force generated during the top layer building is small too. Thus, compressive force from top has little effect on the lower layers. The second is that excessive melting may have occurred in the lower layers due to the heat that was provided when the top layer is built. Numerical analysis and actual measurements of the process are needed to verify these two hypotheses, and they are the subject of future work.

Figure 8 shows a specimen produced by single layer building without a support structure in a previous study [13]. The first part of laser exposed shows a large shrinkage, the last part of laser exposed shows a small shrinkage, and each side is curved. This shape is like the cross section of the bottom layer of the single scan single hatch shown in Figure 7. Figure 9 shows a schematic of the cross section when laminated in each scan strategy based. As the hatching and scanning directions change in each layer, the cross-sectional shape approaches a square. These shapes are similar to the cross section of the bottom layer (0.1mm height) for each scan strategy shown in Figure 7. Thus, it is clear that the cross-sectional shape of the bottom is influenced by the layer built on top.

The difference in shrinkage in the *x* and *y*-directions shown in Figure 6 represents dependence of the laser scan direction of shrinkage. Because the scanning and hatching directions of each layer are orthogonal to each other, the result of the cross scan and reverse hatch is direction independent. Furthermore, the influence of the scan strategy from Figure 6 on the shrinking behavior of low temperature laser sintering weakens with increasing part height but does not disappear. This is due to suppression of deformation and compressive force between the new and existing layers that is mentioned before and the effect of the shape of cross section by lamination as shown in Figure 9.

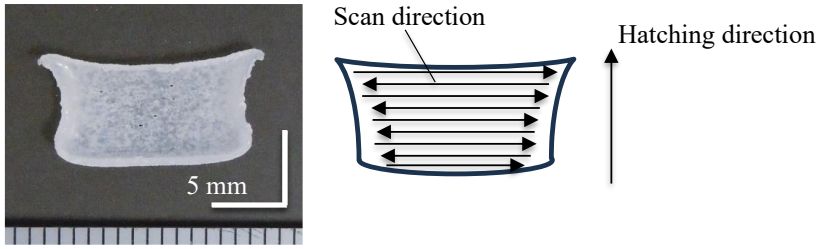

Figure 8. Single layer parts without support structure [13]

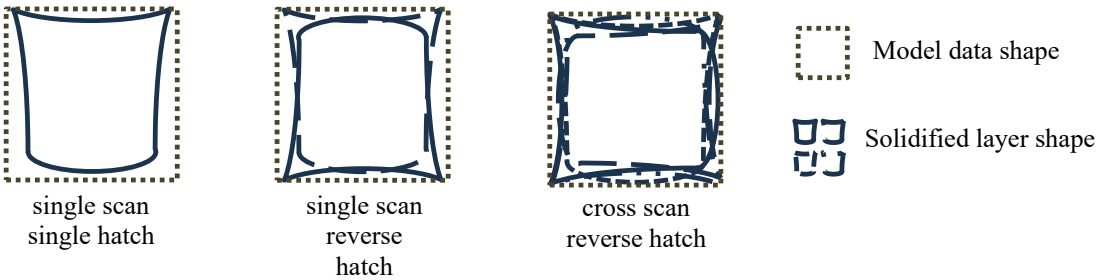

Figure 9. Lamination effect for shrinkage shape in lower part of specimen.

Conclusion

In this study, the shrinkage shape of low temperature laser sintering performed below the recrystallization temperature and the effect of the scan strategy on the shape were investigated. It was found that when a block shaped specimens were made, the upper part of the specimen showed lower shrinkage. In addition, the effect of the scan strategy on shrinkage was observed in the lower height specimens, in the y-direction results, and in the difference between the *x* and *y*-directions. These suggest that the shrinkage shape of single layer and the interaction between layers during the lamination process affect the shrinkage behavior in low temperature laser sintering. This knowledge is an important step in understanding the shrinkage behavior of low-temperature laser sintering and constructing a shape correction model. As the future work, the physical properties and other factors that control shrinkage will be specified and modeled.

Reference

[1] D. L. Bourell, et al., "Performance limitations in polymer laser sintering", Physics Procedia, **56**, 147-156, (2014)
[2] Dotchev et al, "Recycling of polyamide 12 based powders in the laser sintering process," Rapid Prototyping Journal, **15** (2009) 192-203
[3] Josupeit et al. "Material properties of laser sintered polyamide 12 as function of build cycles using low refresh rates", Proc. Solid Freeform Fabrication Symposium 2015, (2015) 540-548
[4] Wudy et al, "Influence of Degradation Behavior of Polyamide 12 Powders in Laser Sintering Process on Produced Parts", AIP Conference Proceedings, **1593** (2014) 691 – 695
[5] T.Niino, et al., Feasibility study on plastic laser sintering without powder bed preheating, Proceedings of the Solid Freeform Fabrication Symposium 2011, (2011) 17-29
[6] T. Kigure, T. Niino, "Improvement of recycle rate in laser sintering by low temperature process", proceedings of annual solid freeform fabrication symposium 2017, 550-556(2017)
[7] T. Kigure, Y. Yamauchi, T. Niino, "Investigation into laser sintering of PEEK using commercially available low powder bed temperature machine", proceedings of annual solid freeform fabrication symposium 2021, (2021)
[8] T. Kigure, Y. Yamauchi, T. Niino, "Relationship between powder bed temperature and microstructure of laser sintered PA12 parts", Proceedings of annual solid freeform fabrication symposium 2019, 827-834(2019)
[9] S. Francesco, et al., "In-situ microwave tomography for parts' cooldown monitoring in powder bed fusion of polymers", Additive Manufacturing, **65**, 103433 (2023)
[10] Y. Yamauchi, T. Kigure, T. Niino, "Quantification of supplied laser energy and its relationship with powder melting process in PBF-LB/P using near-infrared laser", Journal of Manufacturing Processes, **99**, 4, 272-282 (2023)
[11] N. Raghunath, Pandey, P. M. Pulak, "Improving accuracy through shrinkage modelling by using Taguchi method in selective laser sintering", International Journal of Machine Tools and Manufacture, 47, 985-995 (2006)
[12] A. Takezawa, et al., "Simultaneous optimization of hatching orientations and lattice density distribution for residual warpage reduction in laser powder bed fusion considering layerwise residual stress stacking", Additive Manufacturing, **60**, 103194
[13] T. Kigure, Y. Yamauchi, T. Niino, "Relationship between powder bed temperature and microstructure of laser sintered PA12 parts", Proceedings of annual solid freeform fabrication symposium 2019, 827-834(2019)